Kinetics for the Reactions of O^- and O_2^- with $O_2(a^1\Delta_g)$ Measured in a Selected Ion Flow Tube at 300 K

Anthony Midey,[†,‡] Itzhak Dotan,[†,§] S. Lee,[||] W. T. Rawlins,[||] Mark A. Johnson,[+] and A. A. Viggiano*[,†]

Air Force Research Laboratory, Space Vehicles Directorate, 29 Randolph Road, Hanscom Air Force Base, Massachusetts 01731-3010, Institute for Scientific Research, Boston College, Chestnut Hill, Massachusetts 02467, The Open University of Israel, 108 Ravutski Street, Raanana, Israel, 43107, Physical Sciences Inc., 20 New England Business Center, Andover Massachusetts 01810, and Sterling Chemistry Laboratory, Yale University, New Haven, Connecticut 06520-8107

Received: February 15, 2007; In Final Form: March 22, 2007

The kinetics of the reactions of O^- and O_2^- with $O_2(a^1\Delta_g)$ have been studied at 300 K in a selected ion flow tube (SIFT). The $O_2(a^1\Delta_g)$ concentrations have been determined using emission at 1270 nm from the $O_2(a^1\Delta_g, v = 0 \rightarrow X^3\Sigma_g^-, v = 0)$ transition measured with an InGaAs detector calibrated against absolute spectrally dispersed emission measurements. The rate constants measured for O^- and O_2^- are 1.1×10^{-10} and 6.6×10^{-10} cm^3 s^{-1}, respectively, with uncertainties of ±35%. The O_2^- reaction only produces electrons and can be described as Penning detachment, while the O^- reaction has been found to produce both O_2^- and e^-. The O_2^- branching fraction has a lower limit of ∼0.30. Comparison of the present results to previous measurements found in the literature provides a resolution to a previous discrepancy in the rate constant values.

Introduction

Reactions of negative ions that influence electron concentrations help control radiowave propagation in the D-region of the atmosphere.[1] Therefore, these reactions have been among the first reactions studied in the NOAA flowing afterglow system, particularly the detachment reactions of the important D-region ions, O^- and O_2^-, with $O_2(a^1\Delta_g)$.[2] These ions react with ground state O_2 only by very slow clustering. The NOAA group found that these reactions proceed as shown below:

$$O_2^- + O_2(a^1\Delta_g) \rightarrow 2O_2 + e + 51.5 \text{ kJ mol}^{-1} \qquad (1)$$

and

$$O^- + O_2(a^1\Delta_g) \rightarrow O_3 + e + 60.3 \text{ kJ mol}^{-1} \qquad (2)$$

and that reactions 1 and 2 are relatively efficient. The thermochemistry shown above has been calculated from the NIST Webbook values.[3] Consequently, $O_2(a^1\Delta_g)$ production helps tip the balance of negative charge toward electrons in the D-region through these two reactions.

Since that original measurement, a second study has been conducted that found that the rate constants for the O_2^- and O^- reactions are much smaller.[4] Both this study and the NOAA study have been performed in flowing afterglows, and the disagreement between the two is puzzling. Recently, new studies of reaction 2 have also been made by modeling complex O_2 plasmas.[5,6] This more recent determination is in general agreement with the NOAA value.

Further interest in these $O_2(a^1\Delta_g)$ reactions has developed because of their importance in electric oxygen-iodine laser (EOIL) systems. In these systems, the atomic iodine laser transition at 1315 nm, $I(^2P_{1/2} \rightarrow {}^2P_{3/2})$, is excited by energy transfer to atomic iodine from $O_2(a^1\Delta_g)$ produced in an electric oxygen/helium discharge.[7−11] Since O^- is readily formed in such discharges by dissociative attachment of O_2, electron detachment via reaction 2 helps to sustain the discharge.[12,13] Beyond this practical importance, reaction 1 is the only known prototype for Penning detachment, the negative ion analogue of the familiar Penning ionization process between a metastable neutral and another neutral. Electronic energy from the metastable collision partner is used to detach an electron from the other.

Recent advances in $O_2(a^1\Delta_g)$ detection have made it possible to readily study its ion−molecule chemistry in a selected ion flow tube (SIFT). Due to recent advances in thermoelectrically cooled InGaAs photodiodes, $O_2(a^1\Delta_g)$ can now be detected with good sensitivity by observing its emission intensity in the strongly forbidden $a^1\Delta_g \rightarrow X^3\Sigma_g^-$ band at 1270 nm.[11] Problems associated with producing the reactant ions directly in the flow tube of the flowing afterglow are eliminated by using the SIFT. In addition, recent experiments in our laboratory make it possible to quantify possible interferences from O, $O_2(v)$ and O_3 that can be produced during generation of $O_2(a^1\Delta_g)$ by monitoring their ion chemistry.[14−20] As a result, we have undertaken a SIFT study of reactions 1 and 2 to help settle the controversy over the rate constant values. In the process, we have also found a second product channel in the reaction of O^- with $O_2(a^1\Delta_g)$, namely charge transfer, which is shown by eq 3:

$$O^- + O_2(a^1\Delta_g) \rightarrow O_2^- + O - 3.0 \text{ kJ mol}^{-1} \qquad (3)$$

Note that the reaction above is very slightly endothermic and that it has been used to model one of the plasma experiments.[5]

* Corresponding author. E-mail: albert.viggiano@hanscom.af.mil.
[†] Air Force Research Laboratory.
[‡] Boston College.
[§] The Open University of Israel.
[||] Physical Sciences Inc.
[+] Yale University.

10.1021/jp071304b CCC: $37.00
Published on Web 05/25/2007

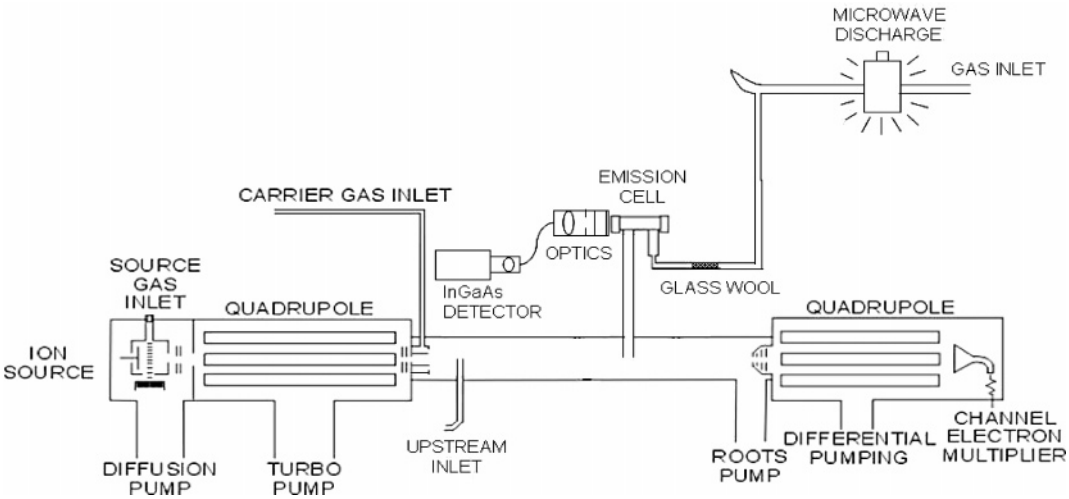

Figure 1. A schematic diagram of the selected ion flow tube (SIFT), including the newly employed quantitative source for $O_2(a^1\Delta_g)$.

Experimental

The measurements were made in the Air Force Research Laboratory's selected ion flow tube (SIFT). This technique for measuring ion−molecule kinetics has been well described previously,[21] and only a brief description of the method is given here, except for a discussion of the measurement of $O_2(a^1\Delta_g)$ concentrations. In short, O^- and O_2^- ions were created from O_2 through electron impact in an external ion source chamber. The ion of interest was mass selected with a quadrupole mass filter and injected into a flow tube through a Venturi inlet. A helium buffer (AGA, 99.995%) carried the ions downstream where $O_2(a^1\Delta_g)$ was added through a Pyrex inlet 49 cm upstream from a sampling nose cone aperture. The primary ions and product ions were monitored by a quadrupole mass analyzer and detected with a particle multiplier. Kinetics were measured by monitoring the ion distribution as a function of $O_2(a^1\Delta_g)$ concentration.

The inlet system for producing and monitoring $O_2(a^1\Delta_g)$ is shown in Figure 1. A fixed flow of He (Middlesex Gases, 99.9999%) and a variable flow of O_2 (Mass. Oxygen, 99.999%) were added to a 0.5 in. o.d. diameter Pyrex tube surrounded by a McCarroll microwave cavity. Producing a microwave discharge of around 25 W created O atoms and $O_2(a^1\Delta_g)$ molecules. However, most of the added O_2 remained in the ground electronic state. The gas mixture then passed through a plug of glass wool to help recombine the O atoms. In past studies of $O_2(a^1\Delta_g)$, a mercury oxide coating on the glass wool was used to speed the recombination process, but safety issues preclude this step in the current arrangement. O atom concentrations were subsequently monitored by the known reactions of SF_5^- and SF_6^- with O as explained later. After passing through the glass wool, the gas mixture entered a 10 cm long Pyrex optical cell with uncoated BK-7 glass windows epoxied at both ends. Emission from $O_2(a^1\Delta_g)$ in the cell is observed via a fiber-coupled optical collection system with a field of view which is well collimated along the length of the cell. An aperture was used so that the cell walls are not in the field of view. The light from the cell is passed through a 5 nm bandwidth interference filter centered on the weak emission from the $O_2(a^1\Delta_g \rightarrow X^3\Sigma_g)$ 0−0 transition at 1270 nm (Andover Corp.). After the filter, the emission is sampled with a 7 mm diameter iris, then focused by a planoconvex BK-7 glass lens (Melles-Griot, LAG 005) into a 24 in. long glass fiber optic cable (SpectraPhysics, 77524). A biconvex BK-7 glass lens focuses the light emerging from the fiber bundle onto a thermoelectrically cooled-InGaAs detector with built-in amplifier (Oriel, 77038). The output of the detector is read by an electrometer (Keithley, 6514) with considerable internal filtering.

Without calibration, this light detection system measures relative $O_2(a^1\Delta_g)$ concentrations. Therefore, the cell, the associated optics and the detector were calibrated at Physical Sciences Inc. using their flow tube $O_2(a^1\Delta_g)$ emission detection scheme. During the calibration, one end of the emission cell was monitored using the AFRL detection system, while the opposite end was monitored by absolute spectrally dispersed emission using a liquid nitrogen-cooled-InGaAs array spectrometer.[11] This device was also fiber-coupled, with a collimated and apertured field of view as described above. The spectrometer acquired the full emission spectrum at 0.4 nm spectral resolution, and was calibrated for absolute intensity using a NIST traceable blackbody source. Analysis of the spectral intensity distributions confirmed that all of the emission was due to $O_2(a^1\Delta_g, v = 0)$, and verified that the rotational temperature was 300 K. $O_2(a^1\Delta_g)$ concentrations were determined by dividing the observed spectrally integrated band intensity by the measured band-averaged Einstein coefficient.[22,23] The setup for generating $O_2(a^1\Delta_g)$ for the calibrations was similar to that on the SIFT reactor, except that the glass wool was absent because the presence of O atoms did not affect the calibration. As a result, the $O_2(a^1\Delta_g)$ concentrations in the cell were considerably larger, providing good signal-to-noise ratios for both the AFRL photometer and the PSI spectrometer. The calibrations consisted of a series of measurements of the $O_2(a^1\Delta_g)$ signal for the photometer versus $O_2(a^1\Delta_g)$ concentration from the spectrometer, for selected pressures, flow rates, and O_2 concentrations at a fixed microwave power.

Two calibration runs were performed at different operating pressures. The results are shown in Figure 2. The $O_2(a^1\Delta_g)$ signal is obtained from the difference between the detector signal obtained with and without O_2 added to the discharge. Good linearity was found between the instruments' response; the two data sets shown in the figure have slopes that are statistically indistinguishable. There is a small offset in the intercept in the lower pressure run, which was attributed to background effects on the small signal levels from the AFRL photometer. The calibration indicates that 1 mV of signal from the AFRL photometer corresponded to 1.72×10^{15} molecules cm^{-3} in the emission cell. Percentages of $O_2(a^1\Delta_g)$ in the total O_2 flow, and the concentrations of $O_2(a^1\Delta_g)$ present in the SIFT were obtained from the calibration curve, the total cell pressure, and the relative

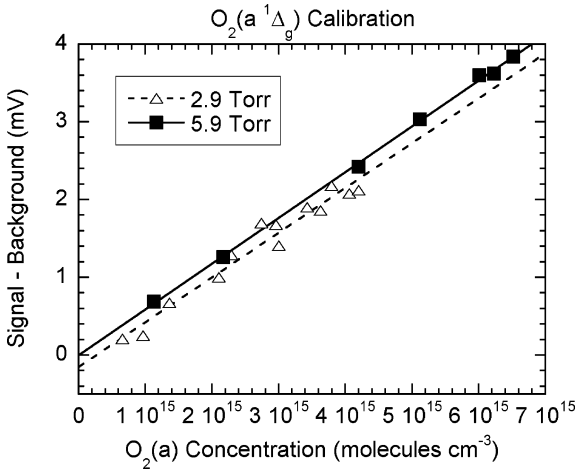

Figure 2. Calibration curve for AFRL $O_2(a^1\Delta_g)$ emission detection scheme. The difference between $O_2(a^1\Delta_g)$ and detector background signals is plotted vs the absolute $O_2(a^1\Delta_g)$ concentration present in the emission cell. See text for details.

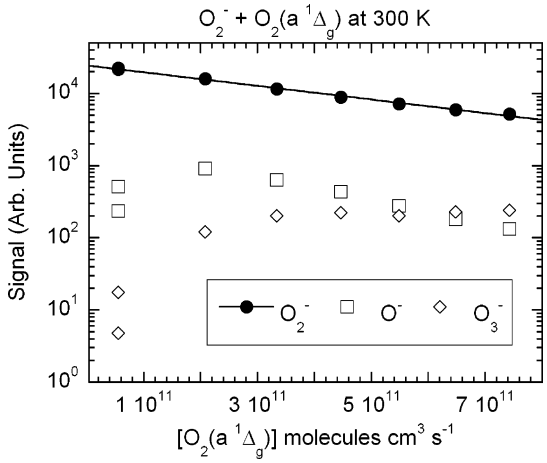

Figure 3. Kinetics data for the reaction of O_2^- with $O_2(a^1\Delta_g)$ at 300 K as measured in the selected ion flow tube (SIFT). The ion signal is plotted vs the concentration of $O_2(a^1\Delta_g)$ in the flow tube. The small O^- and O_3^- signals are the result of reactions of O_2^- with the small amounts O and O_3 impurities that have not been removed. (See text for details.)

He/O_2 flow rates. The small signals detected required relatively long time constants for the $O_2(a^1\Delta_g)$ concentration measurements. Therefore, long kinetic runs were necessary, which sometimes resulted in ion signal drift. To mitigate this situation, a separate determination of the $O_2(a^1\Delta_g)$ concentration versus O_2 flow rate was made and the data were fit to an empirically determined power law. The $O_2(a^1\Delta_g)$ concentrations were then calculated at the end of the kinetics run in order to acquire the data more rapidly and minimize the effects of long-term ion source fluctuations. Periodic checks showed that the fit data were reproducible if the operating conditions were not varied.

The discharge source made O, O_3 and vibrationally excited $O_2(X)$, in addition to $O_2(a^1\Delta_g)$. While the glass wool clearly reduced the O atom concentration, it did not completely eliminate it. SF_6^- and SF_5^- proved to be good ions for monitoring both the O and O_3 concentrations. The chemistry involved was previously measured.[14−17] O_2 did not react with any of the ions used in this study. SF_6^- underwent slow charge transfer with both O and O_3 and SF_5^- reacted with O to produce F^-. No measurable reactivity of either ion with $O_2(a^1\Delta_g)$ was observed. Therefore, the O^-, O_3^-, and F^- signals were used as monitors of the O and O_3 concentrations. Typically, we found that the O, $O_2(a^1\Delta_g)$, and O_3 concentrations were ca. 1%, 9%, and <1% of the O_2 concentration in the flow tube.

The fraction of $O_2(a^1\Delta_g)$ concentration decreased slightly with increasing O_2 flow rate. This effect is a well-known consequence of the decrease in electron temperature and electron-impact excitation rate coefficients in the discharge with increasing diatomic mole fraction.[11,24] $O_2(X, v > 0)$ was monitored by the reaction with O^+. A previous study from our group found that $O_2(v)$ reacted much more rapidly than the ground vibrational state.[18−20] Rate constant measurements for the O^+ reactions with the discharge on and off produced similar values, indicating that: (1) $O_2(v)$ was not present in large concentrations and (2) $O_2(a^1\Delta_g)$ did not greatly increase the rate constant. $O_2(b^1\Sigma_g^+)$ was measured to be much smaller in concentration than $O_2(a^1\Delta_g)$ in such discharge effluent flows, due to much more rapid quenching by O and by collisions with the reactor surfaces.[11] Therefore, only O and O_3 must be accounted for.

The main product channel seen in the current reactions was electron detachment, i.e., electrons were produced by each reaction. In the SIFT, electrons produced in the flow tube by this process diffused rapidly to the walls and the total flux of negative ions to the nose cone decreased as ions were converted into electrons. Thus, monitoring the nose cone current as a function of $O_2(a^1\Delta_g)$ concentration indicated the occurrence of the detachment process.[25]

Results and Discussion

a. Reaction of O_2^- with $O_2(a^1\Delta_g)$. Figure 3 shows kinetics data for the reaction of O_2^- with $O_2(a^1\Delta_g)$. The exponential character of the O_2^- decay is excellent. The small O^- and O_3^- signals are the result of reactions of O_2^- with the small amounts O and O_3 that have not been removed by the glass wool, the latter of which appears to be more important at higher oxygen flows, presumably due to O plus O_2 recombination. An approximately <10% correction to the observed O_2^- rate constant for the O atom reaction has been applied, resulting in a rate constant for reaction 1 of 6.6×10^{-10} cm^3 s^{-1} with a ± 35% uncertainty. This uncertainty is slightly larger than the standard uncertainty[21] of ± 25% because of the additional uncertainty in measuring the $O_2(a^1\Delta_g)$ concentration. The value is an average of four runs with scatter on the order of 10%. The Langevin collision rate constant is 7.35×10^{-10} cm^3 s^{-1}, assuming that $O_2(a^1\Delta_g)$ has the same polarizability as the ground electronic state.[26−28] The bond lengths in the two states are similar, so this assumption should be reasonable. Comparing the observed rate constant to the collision rate constant indicates that the O_2^- reaction is about 90% efficient.

This present value of the O_2^- rate constant is higher than the previous measurements. The NOAA value of $\sim 2 \times 10^{-10}$ cm^3 s^{-1} measured in a flowing afterglow reactor is the closest, although the uncertainty given is a generous factor of 10.[2] However, an erroneously low value for the rate constant could have easily been obtained in the NOAA experiment. O_2^- reactant ions were made by electron attachment to O_2 in the flow tube of a flowing afterglow. Thereby, production of electrons in reaction 1 would be followed by reattachment to the remaining O_2 source gas to recreate O_2^- ions, yielding a slower observed decay and a reduced value for the rate constant. Evidence for this possible interference may be seen in the measurement by Upschulte et al.[4] Figure 6 in that paper shows a kinetic plot with pronounced curvature. The authors accepted the higher flow, slower kinetics part of the graph as indicative of the correct rate constant and they have obtained a value of 2.4×10^{-11} +100%/−50% cm^3 s^{-1}. Fitting their data instead

to a biexponential function shows that the faster decaying part of the curve corresponds to a rate constant of around 2.0×10^{-10} cm^3 s^{-1}, in agreement with the NOAA value. However, the Upschulte et al. measurements also would suffer from the reattachment process. The only way for the present measurements to be consistent with the previous values would be to increase the actual $O_2(a^1\Delta_g)$ concentration by a factor of 3. That would lead to a conversion efficiency of ca. 30%. That value is much higher than expected, especially considering the fact that the glass wool also greatly decreases the fraction of $O_2(a^1\Delta_g)$ entering the emission cell. The calibration experiments at PSI without glass wool had much higher concentrations than those in the kinetics measurements with the glass wool. Therefore, the present value of the rate constant should be correct, intimating that the reaction of O_2^- with $O_2(a^1\Delta_g)$ is extremely efficient.

It is useful to consider the efficiency of reaction 1 from the perspective of its role as an archetypal (and indeed the only, as far as we are aware) example of Penning detachment. Berry[29] has considered this phenomenon from a theoretical perspective and has concluded that these cross sections should be much larger than the neutral analogues, reflecting the long-range capture at play in the ionic encounters. This expectation is thus consistent with the high collision efficiency measured here. In this context, it is also of interest to include the implications of related measurements on the photochemical processes:[30,31]

$$O_4^- + h\upsilon \rightarrow [O_4^-{}^*] \rightarrow O_2(X\ ^3\Sigma_g) + O_2(X\ ^3\Sigma_g) + e^- \quad (4a)$$

$$[O_4^-{}^*] \rightarrow O_2(a\ ^1\Delta_g) + O_2^-(X\ ^2\Pi_g) \quad (4b)$$

which can be viewed as capturing the $[O_4^-{}^*]$ intermediate of reaction 1 at the "half collision". Photoexcitation of O_4^- at 2.37 eV occurs about 1.46 eV above the onset of the electron continuum (reaction 4a), but interestingly results in efficient production of O_2^- exclusively via reaction 4b, which is energetic by 0.98 eV. No ground state $O_2(X^3\Sigma^-)$ is produced in the photodissociation. The photofragmentation channel occurs with a quantum yield of about 30%, indicating that the $O_4^-{}^*$ species, which is deeply embedded in the electron continuum, survives long enough to dissociate into stable products.

More detailed consideration reveals that the collisional and photoexcitation experiments explore somewhat different aspects of the dynamics, as excitation with 2.37 eV photons creates the nascent $O_4^-{}^*$ intermediate about 1.46 eV above the threshold for reaction 4a. This is in a repulsive region of the potential, which is much higher in energy than the region sampled in the (thermal) collisional regime (reaction 1), which is 0.53 eV above the electron threshold. The anisotropic angular distribution of the O_2^- photoproducts (4b) indicates that the photodissociation event occurs with fast, impulsive dynamics, so that the $O_4^-{}^*$ intermediate is only exposed to the electron continuum for on the order of 100 fs. The 30% yield can result from the relative cross sections for excitation of the embedded anion resonance and that of the direct photodetachment continuum, or from competition between the dissociation and autodetachment rates.

While the observation of efficient photofragmentation sets an upper bound on the autodetachment rate, the lower bound is explored by the collision efficiency for reaction 1. The collisional process occurs at much lower energy than that at play in photoexcitation, and samples much larger impact parameters. Both of these effects should lead to much longer lifetimes for the $O_4^-{}^*$ intermediate. In this context, the lower value reported earlier would have implied surprisingly slow $O_4^-{}^*$ electron autodetachment rates (e.g., on the vibrational time scale), while the higher efficiency for collisional detachment (approaching 100%) reported here is consistent with fast autodetachment of the O_4^- intermediate. This may imply that the energy dependence of the efficiency is large. It remains to determine to what extent the 30% photofragmentation quantum yield reflects the amplitude for the production of the two channels as opposed to a reflection of the relative rates of autodetachment and prompt (impulsive) dissociation.

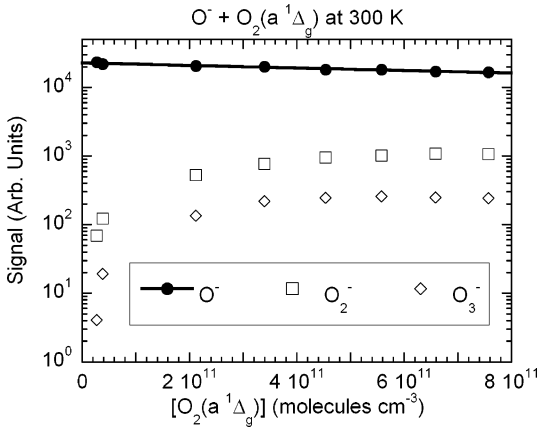

Figure 4. Kinetics data for the reaction of O^- with $O_2(a^1\Delta_g)$ at 300 K as measured in the selected ion flow tube (SIFT). The ion signal is plotted vs the concentration of $O_2(a^1\Delta_g)$ in the flow tube. The small O_3^- signal is the result of reactions of O^- with the small amount of O_3 impurity that has not been removed. (See text for details.)

b. Reaction of O^- with $O_2(a^1\Delta_g)$. Figure 4 shows kinetics data for the reaction of O^- with $O_2(a^1\Delta_g)$. The small O_3^- signal is the result of the reaction of O^- with the small amount of O_3 (<1%) that has not been removed, which appears to be more important at higher oxygen flows. An 18% correction to the observed O^- rate constant for the O atom reaction has been applied. The rate constant for the sum of reactions 2 and 3 is 1.1×10^{-10} cm^3 s^{-1} with an uncertainty of ± 35%. The Langevin collision rate constant is 9.0×10^{-10} cm^3 s^{-1}, indicating that the reaction is only about 10% efficient. The NOAA value for this reaction is 3×10^{-10} +900%/−90% cm^3 s^{-1}. The current measurement is a factor of 3 lower that the NOAA value; however, the rate constants are in agreement within the combined uncertainties of the two experiments. Again, the Upschulte et al. value of 3.3×10^{-11} +100%/-50% cm^3 s^{-1} is much lower. In that reaction, they also showed a curved decay plot and again used the slower portion of the decay as correct, attributing the faster part to reaction with vibrationally excited O_2. If their data are similarly fit with a biexponential function, the faster part of the decay would then correspond to a rate constant of 1.9×10^{-10} cm^3 s^{-1} +100%/−50% cm^3 s^{-1}, in reasonable agreement with the present value. In addition, a recent value derived from modeling of a dc glow discharge yielded the same value, 1.9×10^{-10} cm^3 s^{-1}.[6] An estimate of 1.3×10^{-10} cm^3 s^{-1} for the total rate constant has also been obtained from modeling a radio frequency plasma reactor.[5] Assuming the reanalysis of the Upschulte et al. data is correct, there is general agreement between various measurements within the combined uncertainties of the different methods. Nevertheless, almost a factor of 2 discrepancy remains between the various measurements of the rate constant.

The branching fraction for reaction 3 ($[O_2^-]/([O_2^-] + [e^-])$) has been found to have a lower limit of around 0.27 after the observed O_2^- product counts have been corrected for the contribution from the O^- reaction with the small O_3 impurity.[14] The branching ratios for reactions 2 and 3 are given as limits because the rapid secondary chemistry of O_2^- with O, O_3 and

$O_2(a^1\Delta_g)$ cannot be corrected for completely. The rate constant for reaction 3 only is $\sim 3 \times 10^{-11}$ cm^3 s$^{-1.}$ This pathway is barely endothermic. An upper limit to the rate constant for reaction 3 can be estimated by $k_{col}\exp(-\Delta H/RT)$ to be 3×10^{-10} cm^3 s^{-1}, well above the current value. This channel has not been seen in the previous flowing afterglow experiments, presumably because some O_2^- is present in the initial ion distribution. O^- does not react with $O_2(X)$. Since O^- can be injected cleanly into the SIFT and the increase in O_2^-, seen even after correcting for the O_3 impurity contribution, cannot come from any other species generated in the discharge except $O_2(a^1\Delta_g)$, the current identification of the new reaction product is certain. This finding is significant for application to models of low-pressure oxygen discharge plasmas, since three-body formation of O_2^- is negligibly slow for those conditions, and O^- is commonly thought to be the primary negative ion.[12,13] The likely presence of an energy barrier suggests that the O_2^- channel could become even more important at the elevated temperatures characteristic of such discharges. The presence of this channel has been used to model a radio frequency plasma reactor using a rate constant of 3×10^{-11} cm^3 s^{-1}.[5]

The efficiency of the O^- reaction is only about 10%. One possibility is that there is a hidden quenching channel, i.e., the $O_2(a^1\Delta_g)$ can be converted into $O_2(X)$ efficiently, either by direct quenching or through atom exchange. Neither would be observable in the present system. We are designing a chemical source of $O_2(a^1\Delta_g)$ based on the chemistry used in chemical lasers.[7−11] If successful, it may be possible to look for atom exchange by generating $^{18}O^-$ in the ion source and observing $^{16}O^-$ production. The state of the neutral will still not be detectable. The unwanted O containing species (O, O_3) involved in the present generation of $O_2(a^1\Delta_g)$ makes this too difficult to test here.

Conclusions

The rate constants for the reactions of O_2^- and O^- with $O_2(a^1\Delta_g)$ at 300 K have been measured in a selected ion flow tube (SIFT) using a newly employed emission detection scheme for measuring absolute concentrations of $O_2(a^1\Delta_g)$. O_2^- reacts with $O_2(a^1\Delta_g)$ via electron detachment with a rate constant of 6.6×10^{-10} cm^3 s^{-1}. O^- reacts with $O_2(a^1\Delta_g)$ primarily through electron detachment with a rate constant of 1.1×10^{-10} cm^3 s^{-1}; however, an additional channel producing O_2^- via charge transfer with a branching fraction of ca. 0.27 has also been observed. Discrepancies among the previous literature values can be explained in light of the current results and the limitations of the earlier experiments.

Acknowledgment. We would like to acknowledge Skip Williams for initially generating interest in remeasuring the $O_2(a^1\Delta_g)$ chemistry. Bill McDermott and Steve Davis also provided numerous helpful suggestions on how to handle $O_2(a^1\Delta_g)$. The AFRL portion of this work was supported by the United States Air Force Office of Scientific Research (AFOSR) under Project No. 2303EP4. A.J.M. was supported through Boston College under Contract No. FA8718-04-C-0006. ID was supported under a National Research Council Research Associateship Award at AFRL. Physical Sciences Inc. was supported by funds from AFRL.

References and Notes

(1) In *Handbook of Geophysics and the Space Environment*; Jursa, A. S., Ed.; National Technical Information Service: Springfield, VA, 1985.
(2) Fehsenfeld, F. C.; Albrittion, D. L.; Burt, J. A.; Schiff, H. I. *Can. J. Chem.* **1969**, *47*, 1793.
(3) In *NIST Chemistry WebBook*; NIST Standard Reference Database No. 69; Linstrom, P. J., Mallard, W. G., Eds.; National Institutes of Standards and Technology: Gaithersburg, MD, 2007 (http://webbook.nist.gov).
(4) Upschulte, B. L.; Marinelli, P. J.; Green, B. D. *J. Phys. Chem.* **1994**, *98*, 837.
(5) Stoffels, E.; Stoffels, W. W.; Vender, D.; Kando, M.; Krossen, G. M. W.; de Hoog, F. J. *Phys. Rev. E* **1995**, *51*, 2425.
(6) Belostotsky, S. G.; Economou, D. J.; Lopaev, D. V.; Rakhimova, T. V. *Plasma Sources Sci. Technol.* **2005**, *14*, 532.
(7) Carroll, D. L.; Verdeyen, J. T.; King, D. M.; Zimmerman, J. W.; Laystrom, J. K.; Woodard, B. S.; Richardson, N.; Kittell, K.; Kushner, M. J.; Solomon, W. C. *Appl. Phys. Lett.* **2004**, *85*, 1320.
(8) Carroll, D. L.; Verdeyen, J. T.; King, D. M.; Zimmerman, J. W.; Laystrom, J. K.; Woodard, B. S.; Benavides, G. F.; Kittell, K.; Stafford, D. S.; Kushner, M. J.; Solomon, W. C. *Appl. Phys. Lett.* **2005**, *86*, 111104.
(9) Carroll, D. L.; Verdeyen, J. T.; King, D. M.; Zimmerman, J. W.; Laystrom, J. K.; Woodard, B. S.; Benavides, G. F.; Kittell, K.; Solomon, W. C. *IEEE J. Quantum Electron.* **2005**, *41*, 213.
(10) Carroll, D. L.; Verdeyen, J. T.; King, D. M.; Zimmerman, J. W.; Laystrom, J. K.; Woodard, B. S.; Benavides, G. F.; Richardson, N. R.; Kittell, K. W.; Solomon, W. C. *IEEE J. Quantum Electron.* **2005**, *41*, 1309.
(11) Rawlins, W. T.; Lee, S.; Kessler, W. J.; Davis, S. J. *Appl. Phys. Lett.* **2005**, *86*, 051105.
(12) Franklin, R. N. *J. Phys. D: Appl. Phys.* **2001**, *34*, 1834.
(13) Stafford, D. S.; Kushner, M. J. *J. Appl. Phys.* **2004**, *96*, 2451.
(14) Williams, S.; Campos, M. F.; Midey, A. J.; Arnold, S. T.; Morris, R. A.; Viggiano, A. A. *J. Phys. Chem. A* **2002**, *106*, 997.
(15) Midey, A. J.; Viggiano, A. A. *J. Phys. Chem. A* **2007**, *111*, 1852.
(16) Hunton, D. E.; Viggiano, A. A.; Swider, W.; Paulson, J. F.; Sherman, C. *J. Geophys. Res.* **1987**, *92*, 8827.
(17) Huey, L. G.; Hanson, D. R.; Howard, C. J. *J. Phys. Chem.* **1995**, *99*, 5001.
(18) Hierl, P. M.; Dotan, I.; Seeley, J. V.; Van Doren, J. M.; Morris, R. A.; Viggiano, A. A. *J. Chem. Phys.* **1997**, *106*, 3540.
(19) Viggiano, A. A.; Williams, S. Ion-Molecule Kinetics at High Temperatures (300−1800K): Derivation of Internal Energy Dependences. In *Advances in Gas Phase Ion Chemistry*; Adams, N. G., Babcock, L. M., Eds.; Academic Press: New York, 2001; Vol. 4, p 85.
(20) Mishin, E. V.; Burke, W. J.; Viggiano, A. A. *J. Geophys. Res.* **2004**, *109*, A10301.
(21) Viggiano, A. A.; Morris, R. A.; Dale, F.; Paulson, J. F.; Giles, K.; Smith, D.; Su, T. *J. Chem. Phys.* **1990**, *93*, 1149.
(22) Newman, S. M.; Lane, I. C.; Orr-Ewing, A. J.; Newnham, D. A.; Ballard, J. *J. Chem. Phys.* **1999**, *110*, 10749.
(23) Lafferty, W. J.; Solodov, A. M.; Lugez, C. L.; Fraser, G. T. *Appl. Opt.* **1998**, *37*, 2264.
(24) Rawlins, W. T.; Caledonia, G. E.; Armstrong, R. A. *J. Chem. Phys.* **1987**, *87*, 5209.
(25) Van Doren, J. M.; Viggiano, A. A.; Morris, R. A.; Miller, A. E. S.; Miller, T. M.; Paulson, J. F.; Deakyne, C. A.; Michels, H. H.; Montgomery, J. A. Jr. *J. Chem. Phys.* **1993**, *98*, 7940.
(26) Langevin, P. *Ann. Chim. phys.* **1905**, *5*, 245.
(27) Miller, T. M. Atomic and Molecular Polarizabilities. In *CRC Handbook of Chemistry and Physics*; Lide, D. R., Ed.; CRC Press: Boca Raton, FL, 1995; p 10.
(28) Gioumousis, G.; Stevenson, D. P. *J. Chem. Phys.* **1958**, *29*, 294.
(29) Berry, R. S. *Phys. Chem. Chem. Phys.* **2005**, *7*, 289.
(30) Sherwood, C. R.; Hanold, K. A.; Gerner, M. C.; M., S. K.; Continetti, R. E. *J. Chem. Phys.* **1996**, *105*, 10803.
(31) Han, C. C.; Johnson, M. A. *Chem. Phys. Lett.* **1992**, *189*, 460.